Time-Multiplexed Pulse Shaping

Introduction

Optical pulses are used to transmit information, perform remote sensing and metrology, and study physical processes in matter. These optics and photonics applications require the generation of pulses with control of their temporal characteristics, i.e., instantaneous power, timing, phase, and frequency variations over the pulse shape. Numerous techniques can be used to generate high-bandwidth optical waveforms.[1–8] Direct time-domain generation using high-bandwidth modulators is common in telecommunication applications and has benefited from the progress of high-bandwidth, direct-digital-signal synthesis and amplification. Commercial arbitrary waveform generators (AWG's) with an analog bandwidth higher than 10 GHz, sampling rates up to 65 GS/s, and a sampling depth of 8 bits can be used to drive electro-optic modulators and generate high-resolution optical waveforms.[9,10]

The precise generation of shaped optical waveforms is paramount to high-energy lasers that must deliver on-target pulse shapes optimized for laser–matter interaction. The front end of these facilities must generate optical pulses with low relative jitter and high-bandwidth pulse-shape control. The National Ignition Facility (NIF) (192 high-energy beams) uses 48 AWG's to precisely shape 48 seed pulses sent along distinct optical paths that include optical amplification, frequency conversion, beam smoothing, and focusing.[11,12] Full deployment of the Laser Mégajoule Facility (240 high-energy beams) will require 60 pulse-shaping units to precisely shape 60 seed pulses.[13]

This article presents a time-multiplexed pulse-shaping (TMPS) system generating up to eight synchronized optical waveforms that can be sent to eight distinct optical systems, e.g., sequences of optical amplifiers. A single pulse-shaping unit composed of an AWG and an electro-optic modulator generates a waveform composed of the shaped optical waveforms in different time slots. These waveforms are demultiplexed by a precisely calibrated $LiNbO_3$ 1×8 demultiplexer and then retimed. The use of a common pulse-shaping system significantly decreases the relative jitter between output waveforms, resulting in a significant cost reduction. The OMEGA Laser System now uses a single high-bandwidth AWG and a TMPS system to generate three high-resolution shaped pulses that can be propagated in different amplification systems.[14] The OMEGA EP Laser System will significantly benefit from the implementing a similar pulse-shaping system; in particular, higher-resolution waveforms with lower relative jitter will be generated to seed the four beamlines. A tentative layout for a redesigned fiber front end supporting direct drive on the NIF includes six eight-channel TMPS systems to generate 48 high-resolution shaped waveforms. The following sections describe the principle and implementation of the TMPS system and present experimental results focusing on the performance of the demultiplexer.

Principle and Implementation

1. General System Description

The purpose of time-multiplexed pulse shaping is to generate a plurality of shaped optical waveforms on physically distinct optical paths; for example, optical fibers, using a single high-performance pulse-shaping system [Fig. 146.12(a)]. The pulse-shaping unit generates a composite optical waveform composed of the shaped waveforms in their respective time slots. The composite waveform is sent to an optical demultiplexer configured to route different temporal slices to different outputs. In this work, the demultiplexer is configured to maximize the transmission of time slot j from demultiplexer input to output j while minimizing the transmission of other time slots to the same output. Optical fibers after each demultiplexer output relatively delay the demultiplexed waveforms; for example, when synchronized waveforms must propagate in different sections of a laser system and arrive on target with a predefined relative timing.

TMPS allows for significant performance improvement and cost reduction compared to the implementation of multiple pulse-shaping systems. The relative jitter between the generated waveforms is limited only by the short-term variations of the pulse-shaping system's time base, without any impact from the jitter between the pulse-shaping system and an external trigger. Lowering the relative jitter between waveforms is an important

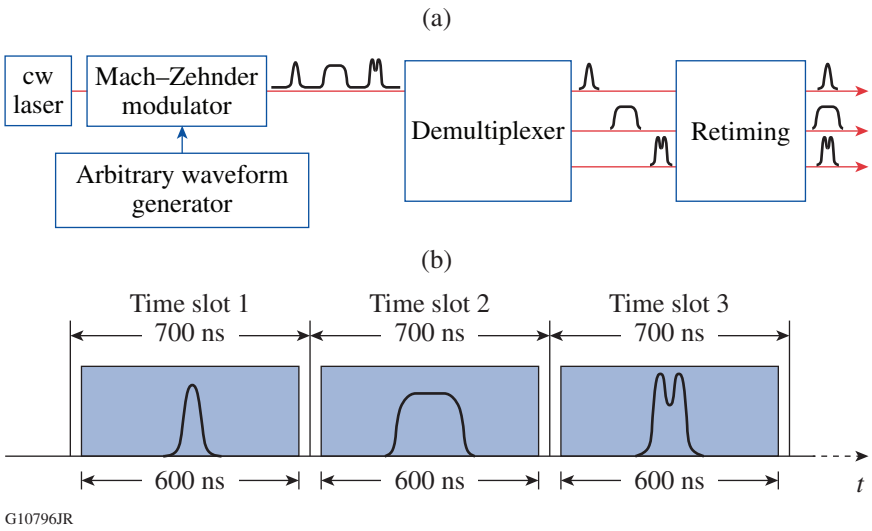

Figure 146.12
(a) Schematic of a time-multiplexed pulse-shaping (TMPS) system. Shaped optical waveforms are generated by modulating a continuous-wave (cw) laser using a Mach–Zehnder modulator driven by an arbitrary waveform generator, demultiplexed, and retimed relative to one another. (b) Timing diagram for the shaped waveforms in the composite waveform generated by the pulse-shaping unit.

consideration when the shaped pulses must be recombined into a single optical waveform later in the system or arrive on target with well-controlled relative timing. Generating multiple shaped optical waveforms with a single pulse-shaping unit instead of several units can significantly reduce the overall cost.

2. Typical Parameters

The required TMPS performance is application dependent. The application we focus on is the seeding of multiple high-energy laser systems. For the seed of each laser system, we allocate a time slot in which the seed pulse can be arbitrarily timed [Fig. 146.12(b)]. This ensures sufficient flexibility to modify the relative timing between seed pulses without reconfiguration or recalibration. In this work, consecutive 700-ns time slots are used because of an operation requirement for OMEGA,[14] where sub-10-ns seed pulses must be temporally tunable by as much as ±300 ns relative to their average timing. The 700-ns slots allow one to tune the seed pulses in a 600-ns range while leaving a 100-ns buffer window for transitioning the demultiplexer between different demultiplexing states.

For an N-channel system (N outputs, N time slots), the demultiplexer performance can be described by the $N \times N$ transmission matrix (T_{ij}), where T_{ij} is the transmission of time slot j from input to output i. Ideally, the diagonal elements are equal to 1 (no loss) and nondiagonal elements are equal to 0 (infinite extinction ratio). In practical conditions (i.e., with insertion losses, demultiplexer and driver imperfections), optimal demultiplexer operation corresponds to maximizing the diagonal elements while minimizing the nondiagonal elements.

3. Demultiplexer Technology

A custom lithium niobate ($LiNbO_3$) waveguide structure composed of fifteen 1×2 $\Delta\beta$ phase-reversal switches[15,16] has been procured from EOSPACE[17] to demonstrate an eight-channel TMPS (Fig. 146.13). In the absence of propagation

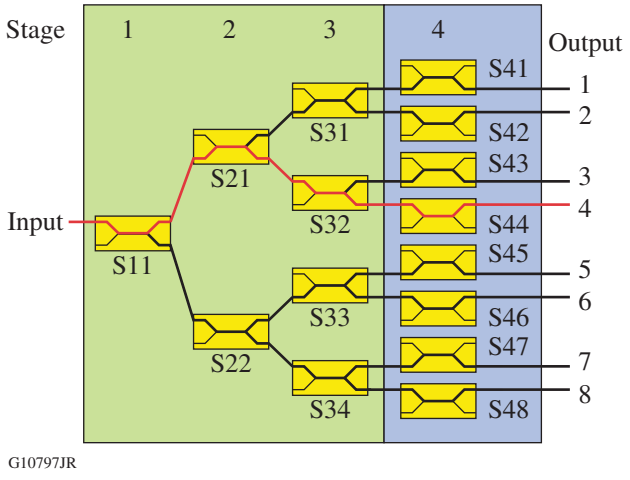

Figure 146.13
Layout of the 1×8 demultiplexer with three demultiplexing stages and one extinction-enhancement stage. Possible optical paths are traced with thick lines. The routing from input to output 4 is traced in red.

losses, the coupling ratio between two adjacent waveguides of length L is described by

$$T_{12} = T_{21} = \frac{1}{1+\left(\Delta\beta L_c/\pi\right)^2}\sin^2\left[\frac{\pi L}{2L_c}\sqrt{1+\left(\Delta\beta L/\pi\right)^2}\right], \quad (1)$$

where $\Delta\beta$ is the difference in propagation constant and L_c is the coupling length. The difference $\Delta\beta$ is controlled by applying a voltage that modifies the local refractive index via the electro-optic effect. Figure 146.14 shows an example of the measured transmission characteristics versus applied voltage for a 1053-nm monochromatic source propagating in a packaged $LiNbO_3$ 1×2 $\Delta\beta$ phase-reversal switch. Two voltages corresponding to the bar (no coupling between waveguides, i.e., $T_{12} = 0$) configuration and cross (all light from each waveguide is coupled to the other waveguide, i.e., $T_{12} \sim 1$) configurations of each 1×2 switch must be identified for optimal routing.

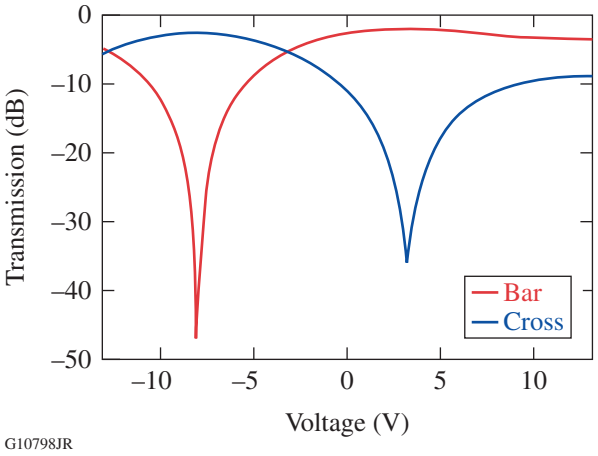

Figure 146.14
Measured transmission from the input to the cross and bar outputs versus voltage for a 1×2 $\Delta\beta$ phase-reversal switch.

The 1×8 demultiplexer designed and fabricated by EOSPACE[17] is organized in four stages (Fig. 146.13):

- Each 1×2 switch in the first three stages (switches S11, S21, S22, S31, S32, S33, and S34) can route its input to either of its outputs for demultiplexing.
- Each switch in the fourth stage (S41 to S48) can route its input to either an output connected to an optical fiber or an unconnected output to enhance the demultiplexer extinction ratio.

4. Driver Technology

To operate the demultiplexer, one must apply control voltages to each of the fifteen 1×2 switches. The most-general driver implementation consists of 15 AWG's that provide a time-dependent voltage to each switch, but this solution is complex, expensive, and cumbersome to integrate. Because demultiplexing requires operating each 1×2 switch in either the bar or cross configuration, a custom driver that produces two independent voltages and switches between them has been designed (Fig. 146.15). The bar and cross voltages are generated by two 12-bit digital-to-analog converters (DAC's) with output voltage between 0 and 5 V, followed by a fast analog switch. An operational amplifier level-shifts and amplifies the analog-switch output to the [–13-V, +13-V] range. A field-programmable gate array (FPGA) drives the fast analog switches. The FPGA uses a 200-MHz clock to specify the state of each analog switch in any 5-ns time window.

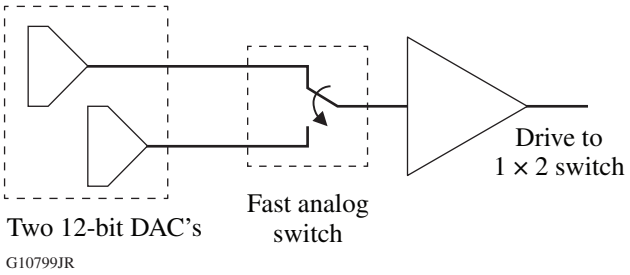

Figure 146.15
Elementary block diagram of the driver for each of the fifteen 1×2 switches in the 1×8 demultiplexer. The field-programmable gate array (FPGA) drives the fast analog switch to produce the voltage value generated by either of the 12-bit digital-to-analog converters (DAC's) and drive the 1×2 switch after amplification.

The state of the 15 analog switches, i.e., the state of each 1×2 switch in the demultiplexer, is defined in a routing table for each output. For example, routing from input to output 4 requires that switch S11 be in the bar configuration, switch S21 in the bar configuration, switch S32 in the cross configuration, and switch S44 in the bar configuration (red path in Fig. 146.13). All other fourth-stage switches are set to the cross configuration to route unwanted light to their unconnected output and enhance the extinction. The FPGA allows for arbitrary demultiplexing patterns, but the switch is sequentially driven for our application, i.e., time slot j is sent to output port j for a given number of cycles of the 200-MHz clock. When externally triggered, the FPGA runs through the defined sequence and waits until the next trigger. The driver and demultiplexer have been successfully operated at trigger rates up to 1 MHz. All results presented here have been obtained at much lower rates (1 kHz

and lower), which are more representative of the operating repetition rates of fiber front ends for high-energy laser systems (300 Hz at LLE and 960 Hz on the NIF).

Experimental Results

1. General Information

The experimental results focus on the performance of the 1×8 demultiplexer supporting the TMPS system at 1053 nm. A trigger and 76-MHz reference signals were provided to the FPGA by a digital-delay generator (Stanford Research DG645) and a waveform generator (Agilent 33250A), respectively. The eight demultiplexer output fibers were connected to fiber-coupled DSC30 photodiodes (Discovery Semiconductors) connected to the two sets of four measurement channels of two 12-GHz oscilloscopes (Agilent). The oscilloscopes record the temporally resolved transmission of the demultiplexer between its input and each of its eight outputs.

In static operation, the voltages applied to the fifteen 1×2 switches are constant and the time-independent transmission between the demultiplexer and its eight outputs is characterized by an 8×8 matrix T_{ij}. This matrix has diagonal elements T_{ii} and nondiagonal elements T_{ij} corresponding to the transmission to output i when the demultiplexer is set to route the input light to output i and to other outputs j, respectively. In dynamic operation, the drives applied to the fifteen 1×2 switches change between their two binary voltage values set by the respective DAC's following a pattern determined by the FPGA. The FPGA keeps the drive voltages constant over time slots of specified duration. When 700-ns time slots are used, the transmission between input and each of the eight outputs is averaged over 600-ns intervals at the center of the eight time slots to quantify the demultiplexing performance because no significant transmission variation was observed in these intervals. This allows one to characterize the demultiplexer performance with an 8×8 matrix for specific dynamic conditions (demultiplexing sequence and time-slot duration). Because of details of the experimental implementation, each line of the transmission matrix in dynamic conditions is scaled to the transmission observed for the diagonal element; therefore, the extinction ratios are defined relative to the outputs.

2. Eight-Channel Static Operation

The demultiplexer is first calibrated with static voltages applied to all fifteen 1×2 switches. The static voltage applied to a specific switch is varied and the transmission between the input and one particular output is measured. The path between input and the chosen output must contain the switch being calibrated (e.g., one can choose output 4 to calibrate switches S11, S21, S32, and S44). This yields 15 transmission curves similar to one of the curves plotted in Fig. 146.14. Each of these curves is fitted with a second-order polynomial around its respective minimum and maximum to identify the optimal operation voltages. This calibration leads to the 30 optimal DAC voltages for static routing between input and outputs by the 15 switches.

The static transmission properties of the calibrated demultiplexer were characterized using a high-dynamic-range power meter. With the power meter connected to output i, the driver was sequentially configured to send light to each output j, therefore leading to a measurement of the transmission T_{ij} after normalization by the input power. The measured transmission matrix T_{ij} (Fig. 146.16) has diagonal elements, i.e., insertion losses, ranging from –4.6 to –5 dB and nondiagonal elements ranging from –55 dB to –70 dB, the latter being the measurement detection limit.

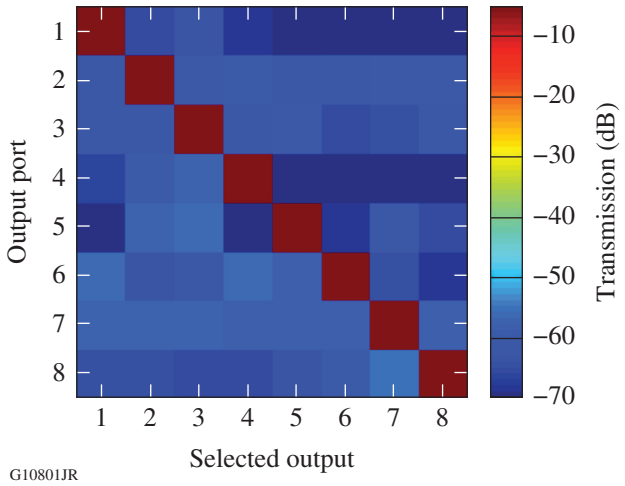

Figure 146.16
Transmission matrix on a logarithmic scale for eight-channel static operation. The transmission is measured at the eight output ports (vertical axis) when the multiplexer is driven to route light to each of the eight ports (horizontal axis).

3. Eight-Channel Dynamic Operation

When the voltage driving a 1×2 switch quickly changes between two different values, e.g., the values corresponding to the bar and cross configurations, the time-resolved switch transmission has a fast component and a slow component. The fast component measured on our system is of the order of 5 ns, including the response time of the custom driver. The slow component is, in comparison, extremely slow (hundreds of microseconds). The existence of these two components implies that drive voltages optimized for static routing are not optimal for dynamic demultiplexing. Non-optimal voltages

increase the insertion losses and decrease the extinction ratios. Drive voltages must be calibrated in dynamic operation, i.e., when driving the demultiplexer to route different time slots (with ~μs duration) of the input signal to different outputs. A general formalism has been developed to ensure that the calibration process is computationally efficient and exhaustive. For a particular switch, the temporally resolved demultiplexer outputs are measured and processed to identify the two drive voltages that optimize the switch transmission in dynamic operation. Optimization consists in maximizing transmission for combinations of time slots and output ports where it must be high and minimizing transmission for combinations of time slots and output ports where it must be low.

The demultiplexer was optimized for dynamic operation with eight output channels. The optimal voltages for dynamic operation were found to be significantly different from the optimal static voltages. The 8×8 transmission matrix with these voltages is shown in Fig. 146.17(a). The lowest observed extinction is –46 dB, and all but five out of the 56 nondiagonal elements of the extinction matrix are lower than –50 dB. For comparison, the eight-channel TMPS system has been characterized when using the drive voltages optimized for static routing [Fig. 146.17(b)]. The observed performance degradation confirms that adequate operation in dynamic operation can be obtained only by calibration in dynamic conditions. The transmission properties of the demultiplexer driven with the optimized static voltages are clearly seen in the resulting time-resolved signals measured on the eight output ports (Fig. 146.18).

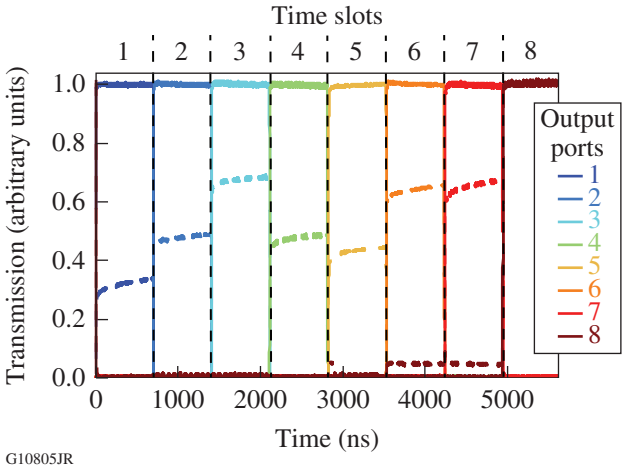

Figure 146.18
Time-resolved transmission measured on the eight output ports in dynamic operation. The continuous and dashed lines correspond to the transmission measured with voltages optimized in dynamic operation and static operation, respectively.

Conclusions

A system architecture to efficiently extend the performance of a single pulse-shaping unit by high-performance demultiplexing has been described. The time-multiplexed pulse-shaping concept generates multiple waveforms in different time slots that are demultiplexed and retimed relative to one another. An experimental implementation of the demultiplexing subsystem based on a 1×8 $LiNbO_3$ demultiplexer based on four stages of 1×2 $\Delta\beta$ phase-reversal switches has been described

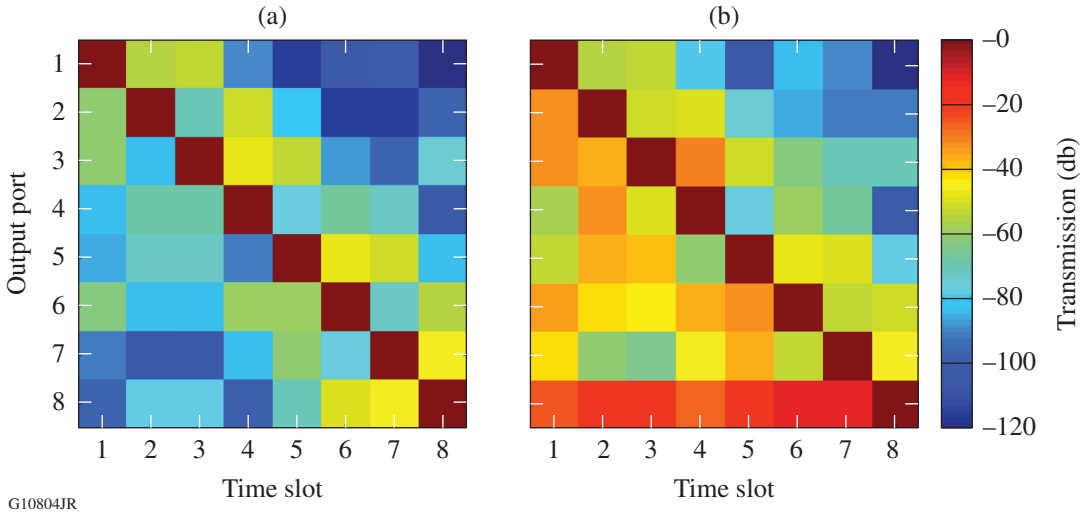

Figure 146.17
Transmission matrix on a logarithmic scale for eight-channel dynamic operation with voltages optimized for (a) dynamic operation and (b) static operation.

and characterized. High-performance demultiplexing has been demonstrated for an eight-channel system (50-dB extinction ratio) by determining optimal values of the drive voltages for each 1×2 switch for dynamic routing.

The demultiplexer was optimized for four-channel operation to support its deployment on OMEGA and OMEGA EP. When demultiplexing of the input waveform to only four output ports is required, the third-stage switches can be used to enhance the extinction ratio of the demultiplexed waveforms. This has led to a measured contrast of the order of 70 dB in dynamic conditions. Operation of the demultiplexer on signals generated at 1064 nm with drive voltages optimized for operation at 1053 nm has led to no significant performance degradation, indicating that the demultiplexer can operate with tunable signals and signals with an optical spectrum broadened by phase modulation.

ACKNOWLEDGMENT

The authors thank G. Kick, R. Hopf, and D. Hassett (Laboratory for Laser Energetics) for their work on the switch driver, and G. Abbas and S. Thaniyavarn (EOSPACE) for fruitful discussion about the demultiplexer. This material is based upon work supported by the Department of Energy National Nuclear Security Administration under Award Number DE-NA0001944, the University of Rochester, and the New York State Energy Research and Development Authority. The support of DOE does not constitute an endorsement by DOE of the views expressed in this article.

REFERENCES

1. A. M. Weiner, Rev. Sci. Instrum. **71**, 1929 (2000).
2. T. Yilmaz *et al*., IEEE Photonics Technol. Lett. **14**, 1608 (2002).
3. P. K. Kondratko *et al*., IEEE Photonics Technol. Lett. **17**, 2727 (2005).
4. A. Monsterleet *et al*., Electron. Lett. **41**, 332 (2005).
5. J. Yao, F. Zeng, and Q. Wang, J. Lightwave Technol. **25**, 3219 (2007).
6. Z. Jiang *et al*., IEEE J. Quantum Electron. **43**, 1163 (2007).
7. Y. Dai and J. Yao, J. Lightwave Technol. **26**, 3329 (2008).
8. M. Bolea *et al*., IEEE Photonics Technol. Lett. **23**, 618 (2011).
9. Arbitrary Waveform Generation Model No. AWG70001A, Tektronix, Inc., Beaverton, OR 97077, http:/www.tek.com (24 May 2016).
10. Keysight Technologies, Inc., Santa Rosa, CA 95403-1738, http://www.keysight.com/main/home.jspx?cc=US&lc=eng (21 April 2016).
11. P. J. Wisoff *et al*., Proc. SPIE **5341**, 146 (2004).
12. C. A. Haynam *et al*., Appl. Opt. **46**, 3276 (2007).
13. J.-F. Gleyze *et al*., Proc. SPIE **7916**, 79160I (2011).
14. T. Z. Kosc, J. H. Kelly, E. M. Hill, C. Dorrer, L. J. Waxer, and W. R. Donaldson, Proc. SPIE **9345**, 93450H (2015).
15. H. Kogelnik and R. Schmidt, IEEE J. Quantum Electron. **12**, 396 (1976).
16. S. Thaniyavarn, Proc. SPIE **578**, 192 (1985).
17. EOSPACE, Inc., Redmond, WA 98052, http://www.eospace.com (17 May 2016).